PNAS RESEARCH ARTICLE | CELL BIOLOGY OPEN ACCESS

Scanning electron microscopy of human islet cilia

Alexander J. Polino[a], Sanja Sviben[b], Isabella Melena[c], David W. Piston[a], and Jing W. Hughes[a,c,1]

Edited by Melanie Cobb, The University of Texas Southwestern Medical Center, Dallas, TX; received February 14, 2023; accepted April 12, 2023

Human islet primary cilia are vital glucose-regulating organelles whose structure remains uncharacterized. Scanning electron microscopy (SEM) is a useful technique for studying the surface morphology of membrane projections like cilia, but conventional sample preparation does not reveal the submembrane axonemal structure, which holds key implications for ciliary function. To overcome this challenge, we combined SEM with membrane-extraction techniques to examine primary cilia in native human islets. Our data show well-preserved cilia subdomains which demonstrate both expected and unexpected ultrastructural motifs. Morphometric features were quantified when possible, including axonemal length and diameter, microtubule conformations, and chirality. We further describe a ciliary ring, a structure that may be a specialization in human islets. Key findings are correlated with fluorescence microscopy and interpreted in the context of cilia function as a cellular sensor and communications locus in pancreatic islets.

primary cilia | human islets | scanning electron microscopy

Significance

Primary cilia are vital cell-surface sensory organelles, but their physical dimensions have eluded characterization due to difficulty in isolating and studying these enigmatic structures, especially in human tissues. In the present study, we use a multi-scale surface scanning approach to enable a 3D architectural study of human primary cilia, the first in pancreatic islets and in any human tissue. Results provide a morphometric basis for understanding ciliary function including signaling capacity, axonemal motility, and cell-cell communication.

Primary cilia are antenna-like sensory organelles that extend from the centriole and project into the extracellular space, serving important functions in sensory detection and signaling. Since their initial description by electron microscopy (EM) in the rodent pancreas (1, 2), primary cilia have been increasingly examined for their link to human metabolic disease, where altered cilia expression or function disrupt pancreatic development and glucose homeostasis (3–7). The pancreatic islets of Langerhans are spherical clusters composed of multiple endocrine cell types. Most cells in the islet, as in the rest of the body, project a single primary cilium, its structure most definitively studied by EM (8–12) in addition to targeted protein staining by immunohistochemistry. In human islets, primary cilia were first described in beta cells, in 1964 in a case of insulinoma (13), whereas validation in nondiseased islet tissues took decades to follow (14–16). More recently, islet primary cilia were found to have glucose- and ATP-regulated motility (16, 17), suggesting that primary cilia are not simply static sensory organelles. These findings have fueled growing interest in islet primary cilia in diabetes research, paralleled by an increasing need to understand the basic structure and composition of these cellular projections. What are their shape and size? What is the mechanical basis for their movement? How might their signaling be compartmentalized? Toward answering these questions, we first aimed to determine the physical parameters of islet primary cilia.

Structurally, primary cilia are divided into several subdomains that are conserved among species and cell types. Lengthwise, cilia are composed of a basal body and an axoneme. The basal body is the mother centriole of the cell, a microtubule-based cylinder that emanates from near the Golgi and remains entirely intracellular. It anchors the primary cilium via a connecting transition zone, a morphologically distinct segment that projects out of the ciliary pocket and controls cargo trafficking to the axoneme. The primary cilia axoneme has a highly conserved conformation of nine outer microtubule doublets with a lack of central microtubules, hence named "9 + 0," a pattern consistently observed at the axonemal base and thought to continue through the length of the cilium. This model has required revision, however, due to reports of non-9+0 cilia cross-sections captured by transmission electron microscopy (TEM) as well as 3D tomography of primary cilia in cells of both pancreatic and nonpancreatic origin (9, 18–22). The updated view is that the canonical ciliary "9 + 0" configuration changes soon after leaving the cell body, and that microtubule number and arrangement may be modified along the length of the cilium. We recently reported on the non-9+0 arrangement of human islet cilia, but only in sporadic thin sections of resin-embedded tissue prepared for TEM (16), while how the axoneme structure might evolve from base to tip in islets is unknown. Many other morphometric features of human islet primary cilia also remain undefined, including axonemal length and diameter, geometry of microtubule filaments, whether they assemble higher order conformations, and the presence of any accessory components contributing to the maintenance of axonemal integrity, dynamics, and sensory signaling function. Thus, elucidating islet cell cilia structure and especially visualizing the entire axonemal cytoskeleton is a priority in islet research.

Author affiliations: [a]Department of Cell Biology and Physiology, Washington University School of Medicine, Saint Louis, MO 63110; [b]Washington University Center for Cellular Imaging, Washington University School of Medicine, Saint Louis, MO 63110; and [c]Department of Medicine, Washington University School of Medicine, Saint Louis, MO 63110

Author contributions: A.J.P., D.W.P., and J.W.H. designed research; A.J.P., S.S., I.M., and J.W.H. performed research; S.S., D.W.P., and J.W.H. contributed new reagents/analytic tools; I.M. and J.W.H. analyzed data; and J.W.H. wrote the paper.

The authors declare no competing interest.

This article is a PNAS Direct Submission.

Copyright © 2023 the Author(s). Published by PNAS. This open access article is distributed under Creative Commons Attribution-NonCommercial-NoDerivatives License 4.0 (CC BY-NC-ND).

[1]To whom correspondence may be addressed. Email: jing.hughes@wustl.edu.

Published May 19, 2023.

Advances in superresolution and electron microscopy combined with increasing availability of human donor specimens makes it now possible to perform ultrastructural studies on primary human islets. Large open-access databases such as the nPOD nanotomy atlas have curated scanning transmission EM images of human islets (23). While these images are useful for demonstrating disease-related morphological alterations across cellular compartments, cilia and centrosomes were not examined in these studies owing to their rarity and low likelihood of identification. To enable ultrastructural characterization of islet primary cilia, we used surface topography imaging by scanning electron microscopy (SEM) to directly visualize the ciliary axoneme in human pancreatic islets. This approach allows cilia identification based on their extracellular localization and distinct morphology and preserves full-length cilia structure in situ. We examined cilia with or without demembranation to compare surface versus cytoskeletal details of primary cilia, both contextually within intact human islet tissues (Fig. 1). Ciliary components post-demembranation were preserved with clarity, allowing quantification of microtubule size, number, chirality, and observation of structural motifs not previously described in other mammalian cilia.

Results

We examined individual cilia on 15 islets from three human donors (Table 1). The islets in our study were isolated from human donor pancreata and ranged in size from 100 to 300 μm in diameter, consistent with dimensions reported in literature. Intact islets exhibited round shape and well-preserved surface contour, with the contrasting textures among adjacent cells exhibiting a soccer ball-like appearance (Fig. 2*A*). Primary cilia are prominent structures on the islet surface, typically measuring 3 to 6 μm in length, are flexible and display varying curvature. Other membrane protuberances such as microvilli and filopodia are also observed on the islet surface. The vast majority of human islet cells bear a single cilium each, a feature that we and others have previously demonstrated by immunofluorescence microscopy (14, 16, 24, 25).

In the present study, primary cilia were imaged with or without demembranation, the latter revealing a clear view of the axonemal structure from base to tip. Attrition in cilia number occurred at each step of sample preparation and image acquisition. In total 60 full-length cilia including 50 membrane-extracted and 10 non-extracted samples were selected for morphometric analysis. Multi-scale SEM was used to visualize structural details of each cilium and its subdomains with progressively higher resolution.

Ciliary Length, Diameter, and Volume Estimations. Most cilia on the islet periphery project away from the cell, while some project horizontally along the membrane (Fig. 3). We sought to determine the linear dimensions of islet primary cilia, keeping in mind the caveat that measurements of 3D object length in 2D images are by nature underestimations. By virtue of the object tilt, planar-extrapolated lengths can only be equal to or shorter than actual object length. To achieve the best estimation of ciliary length, we selected mostly cilia that were captured in profile perpendicular to the imaging detector. Average axonemal length measured 5.74 ± 2.3 μm among 50 extracted cilia and 4.21 ± 1.5 μm among 10 unextracted cilia, with comparable distributions (Fig. 3*C*). As human islet cilia are wider at the base than tip, we measured ciliary diameter both proximally and distally, obtaining an average of 237 ± 52 nm at the base and 148 ± 37 nm at the tip for extracted cilia (Fig. 3*D*). These dimensions were similar in unextracted cilia, 240 ± 80 nm at the base and 121 ± 51 nm at the tip. Overall length and diameter measurements were comparable to those determined by cryoelectron tomography (cryo-ET) in cultured kidney cell cilia and those reported for other mammalian cilia (19–21).

Using averaged length and diameter measurements from all cilia, we estimated the human islet primary cilium volume and surface area based on the shape of either a truncated circular cone or a right cylinder (Fig. 3*E*). As a truncated cone with a base and tip diameter of 0.24 and 0.14 μm (radius 0.12 and 0.07 μm) and height of 5 μm, the cilium volume is estimated to be 0.15 μm^3, with a surface area of 3.05 μm^2. As a cylinder, with an average axonemal diameter of 0.2 μm (radius 0.1 μm), the cilium has a volume of 0.16 μm^3 and surface area of 3.2 μm^2. Thus the two model methods are in good agreement with each other.

We next measured the average diameter of single islet cells in our dataset, which was 12 to 14 μm (radius 6 to 7 μm), and determined the cytoplasmic volume to be ~1,000 μm^3. This allowed us to calculate the ratio of cytoplasmic volume to ciliary volume for human islet cells as approximately 6,000 to 7,000. The ratio of plasma membrane surface area to ciliary membrane area is about 150 to 200. These ratios were previously estimated to be 5,000 and 500, respectively, for a typical 0.3 × 5-μm primary cilium (26). The minor discrepancy between our and previous

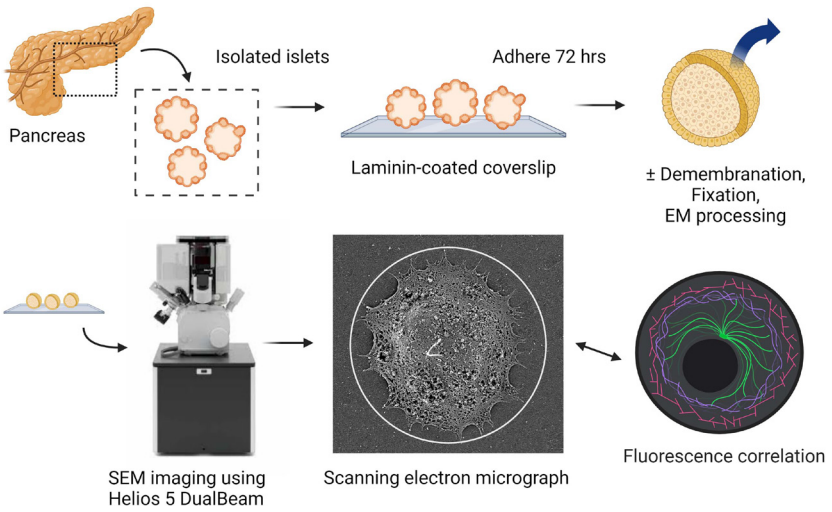

Fig. 1. Scanning EM workflow for visualizing primary cilia on intact human islets.

Table 1. Human islet donor characteristics

Donor	Gender	Age (y)	BMI (kg/m^2)	Diabetes
1	M	54	28.4	No
2	M	32	26.9	No
3	M	16	29.5	No

estimates is due to a smaller diameter of human islet cilia than that generally assumed (0.24 μm versus 0.3 μm at the base). Thus, human islet cilia appear slightly more slender than what is typical for other mammalian primary cilia. Nonetheless, the values we obtained for human islet cilia are comparable to prior estimates from nonislet cells (26, 27), indicating that the physical dimensions of primary cilia are largely conserved across tissues and organisms.

The actual shape of the human islet primary cilia, of course, is not a uniform cone or cylinder. Our SEM imaging revealed remarkable cilia geometries and structural motifs, which we now describe from base to tip. Special attention is given to axonemal domains with known functional importance, as well as previously uncharacterized structural elements.

The Ciliary Pocket and Transition Zone Are Well-Visualized by SEM. The ciliary pocket is an invagination of the plasma membrane from which the primary cilium emanates. It is a specialized domain for ciliary protein trafficking, endocytosis, and actin cable docking, among other functions (28, 29). Ciliary pockets had been observed in mouse islets more than a half century ago by TEM, in beta cells exhibiting deeply rooted cilia where the ciliary pocket was interpreted as a site of basal body docking to the plasma membrane, with a presumed role in primary ciliogenesis (1). In the present study, the ciliary pocket of human islets is seen to form a circular pit surrounding the axoneme in some cells, while in others the cilium erupts from the surface without an appreciable ciliary pocket, and there are other cells still that have such deeply rooted cilia within recesses of the cell that a ciliary pocket is not visible (Fig. 4). From these observations we conclude that the ciliary pocket adopts specialized configurations among different human islet cells, a theme that is consistent with the differential membrane organization at the cilia base that has been described in other systems (28–31).

Higher up, the transition zone is the proximal-most region of the axoneme and is captured in striking clarity in our study. There is a section of 5 to 6 parallel rows of particles that encircle the cilia base orthogonal to the direction of axonemal microtubules (Fig. 4 *B–D*), corresponding to the "ciliary necklace" that has been described at the neck of the cilium in many species, where it supports the microtubule transition from triplets to doublets and acts as a membrane diffusion barrier (32–36). The necklace in human islet cilia measures approximately 230 nm in diameter and 140 nm in height in the visible portion above the cell. Individual bead-like particles comprising the necklace measure approximately 12.5 nm in diameter each, similar to the dimensions of the intramembrane particles previously described for kinocilia in the respiratory epithelium (37). The distance between the necklace rows, or strands, is about 18 to 22 nm, and the number of extracellular strands ranges between 3 and 6 per cilium. Whereas the ciliary necklace had best been previously demonstrated by freeze-etching EM (32, 37), a technique that relies on a carbon cast replica of the structures in study, our imaging approach visualizes the structure itself, allowing direct morphometric measurements of its components.

Distal to the ciliary necklace, we see cylindrical strands of microtubule doublets forming the ciliary axoneme. Small knob-like densities with diameters of ~20 nm are observed

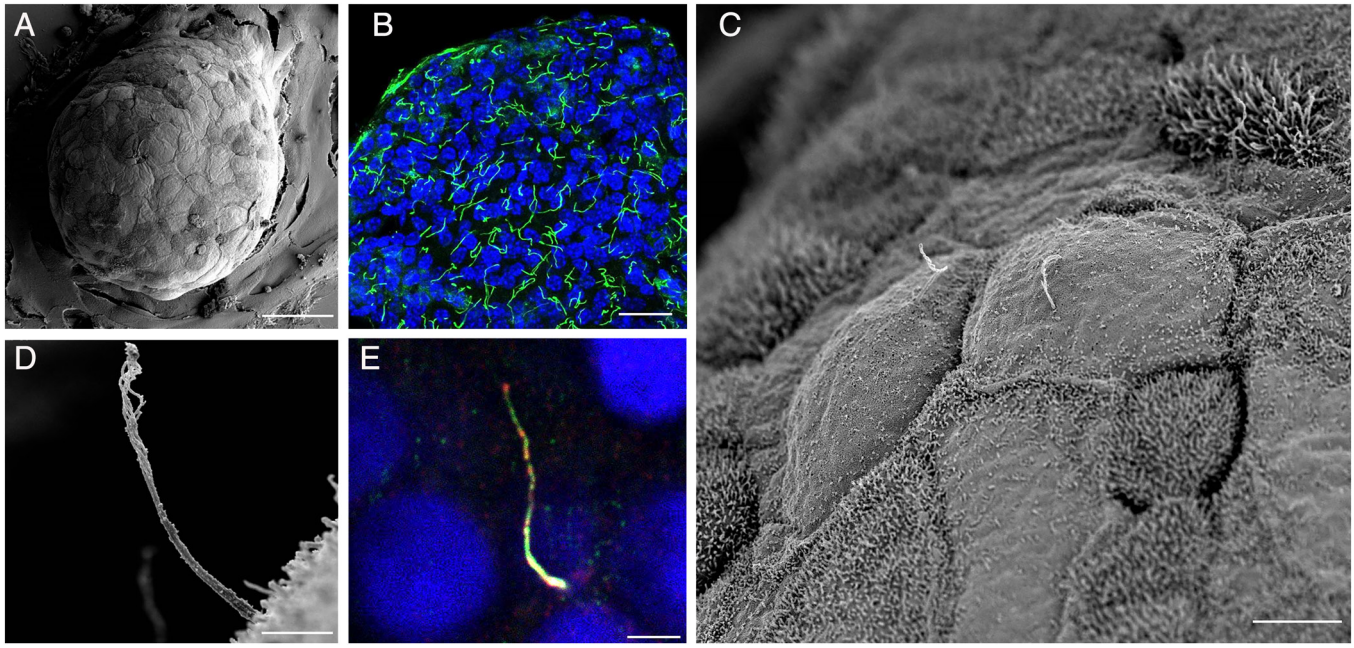

Fig. 2. Multiscale imaging of human islet primary cilia. (*A*) Intact human islets are immobilized on glass coverslips and membrane-extracted to reveal ultrastructural surface details. Shown is an average-sized islet with approximately 100 cells on the exposed surface. (Scale, 50 μm.) (*B*) Confocal image of a human islet single-plane cross-section showing primary cilia in green (acetylated-α-tubulin) and nuclei in blue (DAPI). (Scale, 20 μm.) (*C*) Higher-resolution view of an islet region showing two centrally located cells projecting primary cilia. Surface texture differs among adjacent cells depending on the presence or absence, and length, of microvilli. (Scale, 10 μm.) (*D*) A full-length cilium is captured in profile on the islet surface, showing evolving morphology from proximal to distal segments. (Scale, 2 μm.) (*E*) A human islet cilium labeled by cilia markers ARL13b (red) and axonemal dynein DNAI1 (green), showing comparable cilia length, width, and curvature as those in SEM images. (Scale, 2 μm.)

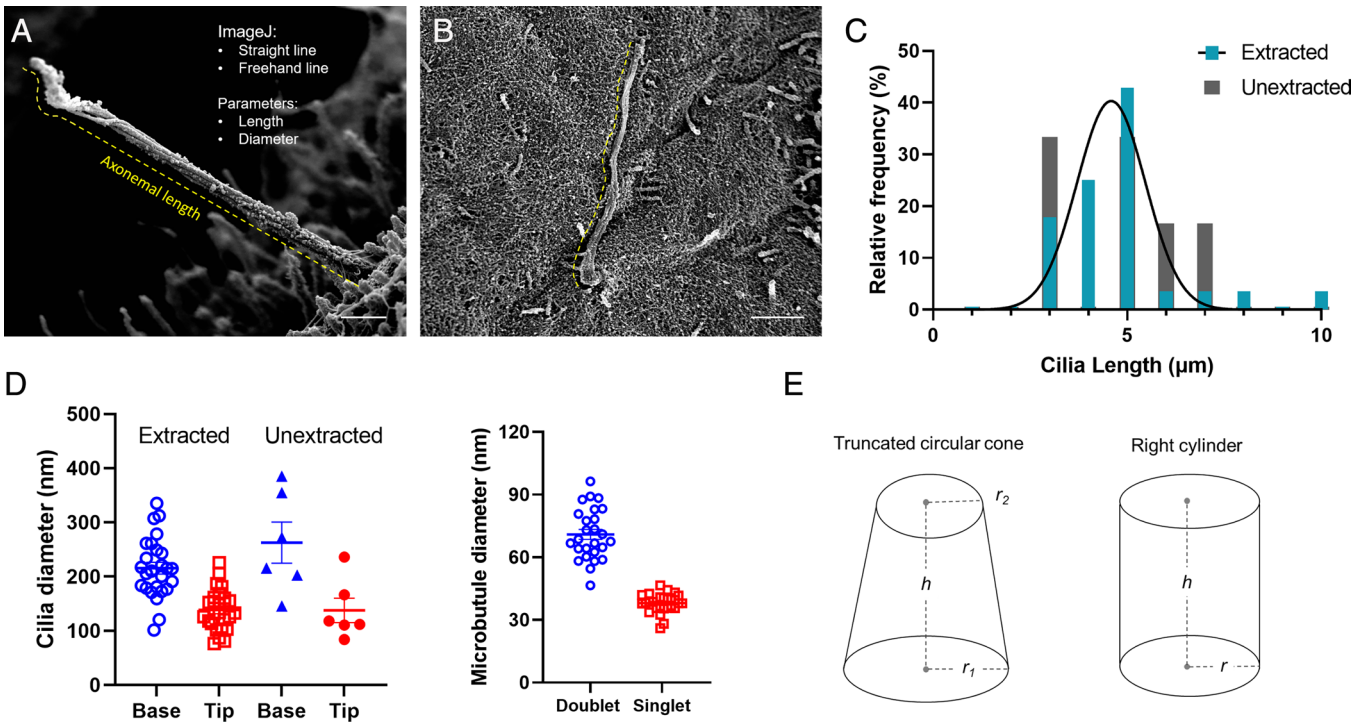

Fig. 3. Cilia length measurements at the islet surface. Full-length cilia with intact tips are used for axonemal length determinations. (*A*) A cilium projecting away from the islet surface with a relatively straight axoneme, whose length can be traced using a combination of the straight line and freehand line tool in ImageJ, shown in yellow dash. Cross-axonemal diameters are measured using a straight line tool at the cilia base and tip. (Scale, 500 nm.) (*B*) A curvy cilium along the islet surface, whose length is best estimated using the freehand line trace tool. (Scale, 2 μm.) (*C*) Morphometric analysis of human islet cilia showing distribution of axonemal length among 60 primary cilia including n = 50 extracted, 10 unextracted. (*D*) Diameter measurements at the cilia base and tip, as well as microtubule doublet and singlet diameters measured in extracted samples only. Bars represent mean ± SD. (*E*) Geometric approximations of primary cilia for volume and surface area calculations, *r*, radius; *h*, height.

decorating the microtubules and are similar in size and shape as the beads that constitute the ciliary necklace (Fig. 4). These particles are also present on microvilli and cortical cytoskeleton, in a dense albeit irregular way, thus appear nonspecific to cilia and may represent membrane remnants or debris postextraction and postfixation. Occasional larger appendages are seen to associate with the axoneme surface (Fig. 5*A*), but we did not observe regular repeats of polymer complexes resembling intraflagellar transport trains (19, 38), which may not have survived demembranation.

Cilia Are Tethered by Microfilaments at the Base. We observe physical interactions between the ciliary axoneme and ciliary pocket as well as with the cell surface. The base of the primary cilium is connected by thin filaments to the surrounding microvilli and cytoskeleton surface (Figs. 4 *A*–*C* and 5 *A* and *B*). These microfilaments have a diameter of 7 to 10 nm and a branching form, consistent with actin fibers which are known to associate with primary cilia—particularly at the base (28, 39–41). Location and morphology-wise, they are distinct from the Y-links in the transition zone of cilia and flagella (21, 32, 38, 42, 43), which are symmetrically present on all microtubules and serve to tether the microtubules to the ciliary membrane. In contrast, these external filamentous strands observed in our study are located above the transition zone, attach to distant targets including neighboring microvilli and cell surface, and are asymmetrically arranged around the axoneme, predominating on one side of the cilium (Fig. 4 *A* and *B*). Similar filaments are also present on microvilli, where they are more symmetrically distributed and create an aster-like network. Neither cilia- nor microvilli-associated filaments are visible in nondemembranated samples (Fig. 5 *C* and *D*), suggesting that these structures are normally sheathed by the ciliary and plasma membranes. Fluorescence imaging of mouse islets using structured illumination microscopy provides supporting evidence that the base of islet primary cilia is embedded in an F-actin network (Fig. 5 *E* and *F*).

Microtubule Doublet-to-Singlet Transition. In all observed cilia, individual microtubule filaments start as doublets at the cilia base and transition to singlets at the one-third to half-way mark along the axoneme, between 1 and 2 μm from the base, at which point the cilium takes on a noticeable change in diameter and width (Fig. 6). There is a clear demarcation where this change takes place, beyond which point the microtubules become thinner and more loosely associated, reflecting a change in filament organization and intrafilament cross-linking. Such microtubule doublet-to-singlet transitions have been reported in cultured kidney cell cilia (19, 21) and can be observed in open-access volumetric imaging of rodent and human pancreatic islets (20, 22, 23). Direct measurements from our dataset showed that human islet cilia microtubule singlets possess an average diameter of 37 ± 4 nm, approximately half that measured of microtubule doublets (68 ± 10 nm). These numbers are consistent with those previously reported in kidney primary cilia (19, 21). Small globular densities are seen coating the microtubule doublets in the proximal axoneme, whereas they are generally sparse or absent on distal portions of microtubules (Figs. 6 and 7).

Cilia Handedness and Secondary Structure. As microtubule filaments evolve from doublets to singlets, they undergo conformational changes with respect to each other. Whereas they begin as a tight straight bundle in the ciliary basoproximal region, the microtubules begin to separate distally and twist about a central axis before coalescing at the tip (Fig. 7). There is a periodicity to the microtubule rotations, measuring 900 to 1,000 nm in arc length with a pitch of 500 to 1,000 nm between turns. Within the loose microtubule bundle, actin-like thin filaments with a

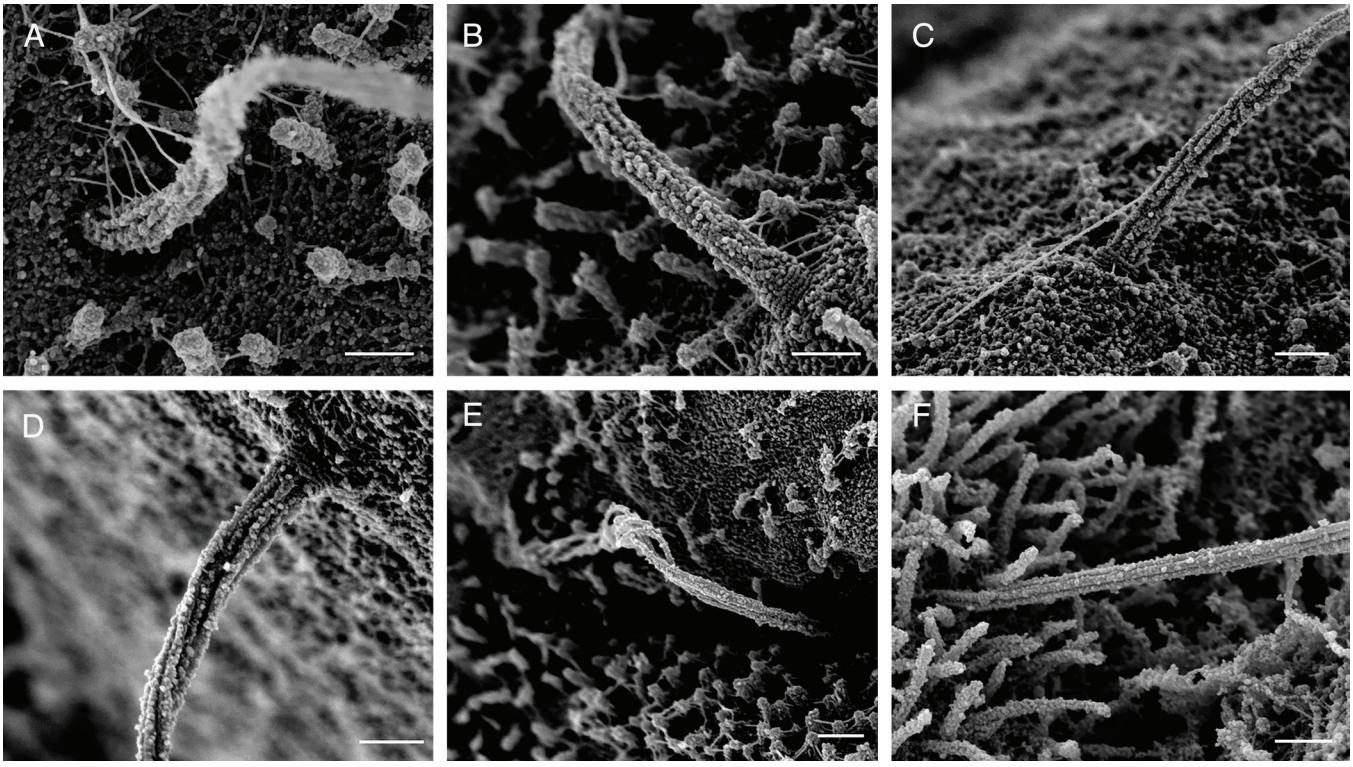

Fig. 4. Heterogeneous morphology at the ciliary base. The proximal region of human islet cilia differs among cells, showing variable depths of ciliary pocket and basal attachments (*A*–*D*) including Y-shaped linkers between the cilium base and nearby surface structures. In some cells, the cilia base is buried within membrane recesses and microvilli and therefore not visualized (*E* and *F*). The ciliary necklace, when exposed, is visualized in exquisite detail (*B*–*D*), revealing discrete rows of transition zone particles perpendicular to the axonemal microtubules. (Scale, 300 nm.)

diameter of ~8 nm are occasionally observed stretching along the long microtubule axis (Fig. 7*C*). Occasional microtubules break or splay apart (Fig. 7 *E* and *F*), likely as a consequence of physical disruptions from extraction and fixation. Given its helical nature, the axoneme is intrinsically chiral. Human islet cilia are predominantly left-handed (>80%), while a minority have a mild right-handedness (~8%), and a similar minority have no discernable rotation (Fig. 8*A*). This is in contrast to the predominant right-handed spins reported for kidney cell cilia (19, 21). To be sure of our observations, we confirmed using fiducial markers that our SEM images are not mirror images. The presence or absence of taxol also did not alter the rotational nature and direction (Fig. 8*B*), suggesting that these higher order microtubule conformations are fairly stable.

A Ciliary Ring Is Occasionally Observed in the Proximal Axoneme. We observe a rare but potentially important feature, which is that a ring is present in the proximal axoneme, at about 1 to 1.5 μm from the base. It wraps around the axonemal bundle as a continuous strand with similar texture and diameter as a microtubule singlet or doublet (30 or 60 nm) (Fig. 9). We name this structure the "ciliary ring" to differentiate it from the ciliary necklace and ciliary bracelet, which are separate structures (32, 44, 45). Rings are observed on 4 out of 50 demembranated cilia (8%) and were present on islets from multiple donors, thus not an isolated phenomenon. All rings occurred on cilia from cells that possessed short microvilli and therefore were likely beta cells. One cilium was observed to bear two rings that subdivide the axoneme into equidistant thirds (Fig. 9 *C*–*E*). Distal to each ring, the axoneme exhibits greater separation and twist, appearing as if the ring is acting as a band to keep the microtubule bundle together. Rings are not observed on unextracted cilia, indicating that the structure occurs submembrane.

Ciliary Tip as a Special Domain. The distal ciliary domain, or tip segment, is captured intact in demembranated islet cells, showing structural organization that differs from the rest of the axoneme. The microtubules decrease in number toward the distal cilium before terminating into a dense cap structure (Fig. 10 *A*–*C*). There is diversity in the number of microtubules that make it to the tip, typically between 3 and 5, but up to 7 have been counted. A greater diversity in cilia tip morphology is seen in nonextracted samples in which the cilium retains its membrane covering, where the enclosed tip shape ranges from pointed to rounded to bulbous (Fig. 10 *D*–*F*). The highly dilated tip seen in Fig. 10*F* resembles those previously described in normal kidney collecting duct cilia (46) as well as cilia bearing mutations affecting retrograde transport that cause a buildup of cargo and vesicles in the tip region (47–49). Our specimens came from healthy donors with no known metabolic disease or ciliopathies, suggesting that these morphological differences may represent a normal spectrum of pancreatic islet cilia in various stages of growth and remodeling. Overall, the unique morphology of the cilia tip observed in our study is consistent with its role as a dedicated sensory and signaling domain, where the diversity of tip structure may be related to specific ciliary roles in different islet cells.

Multiciliated Islet Cells. Occasional compound cilia are observed by SEM where a single cell may project two or even three cilia from the same base. These are rare, estimated <5% frequency among human islet cells. We observed three cases of double cilia and one case of triple cilia. One clear example each is shown in

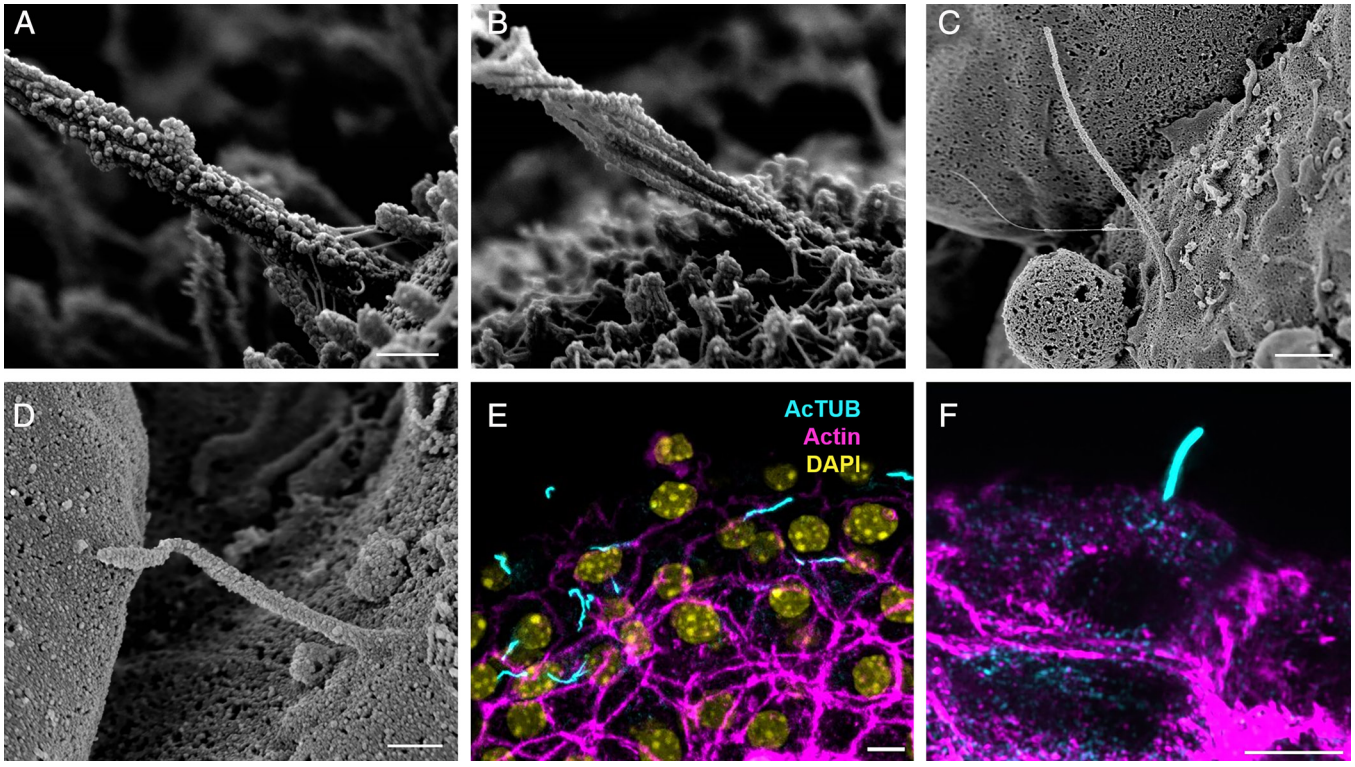

Fig. 5. Actin-like microfilaments attach at the cilium base. Thin filaments connect the base of the cilium to microvilli and the cell surface, with branching patterns seen at the axonemal and microvilli attachment points (*A* and *B*); scale 300 nm. These microfilament tethers are not visible on unextracted cells that have retained their plasma and ciliary membranes (*C* and *D*); scale, (*C*) 1 μm, (*D*) 400 nm. (*E* and *F*) Actin filaments are visualized by phalloidin staining (magenta) at the base of primary cilia (cyan); nuclei (yellow); scale 5 μm, structured illumination microscopy.

Fig. 11 from unextracted cells that had intact cilia membrane. In both cases, the double and triple cilia projected axonemes that were similar in length and diameter and exhibited varying degrees of physical interactions among the axonemes. These project as independent axonemes, analogous to the human dermatologic condition of *pili multigemini* or "tufting" where

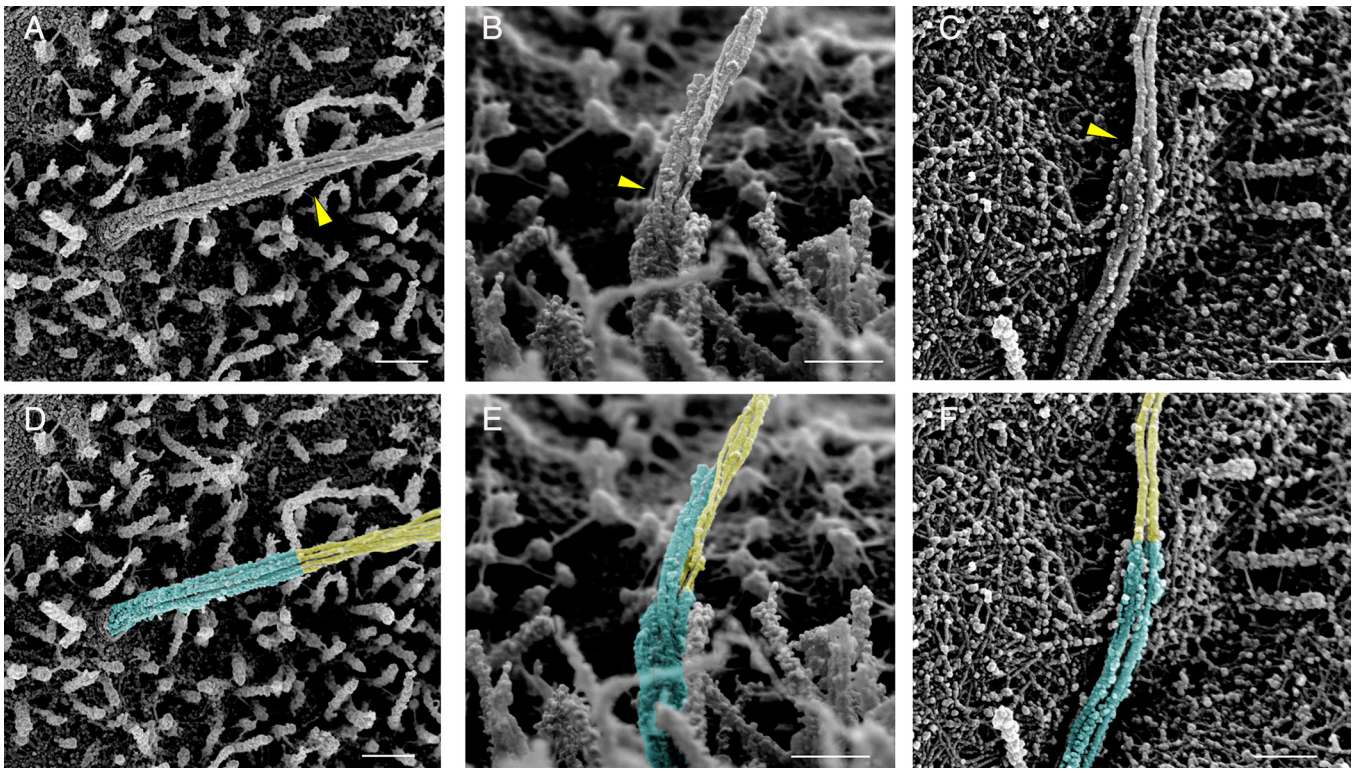

Fig. 6. Microtubule doublet-to-singlet transitions are visible on the axoneme. Representative SEM and false-color images showing the demarcation along the axoneme where microtubule doublets become singlets, resulting in a reduction of microfilament and axoneme diameter. Transition points are marked by yellow arrowheads in (*A*–*C*) and by false-color in (*D*–*F*), cyan corresponding to doublets, yellow singlets. (Scale, 300 nm.)

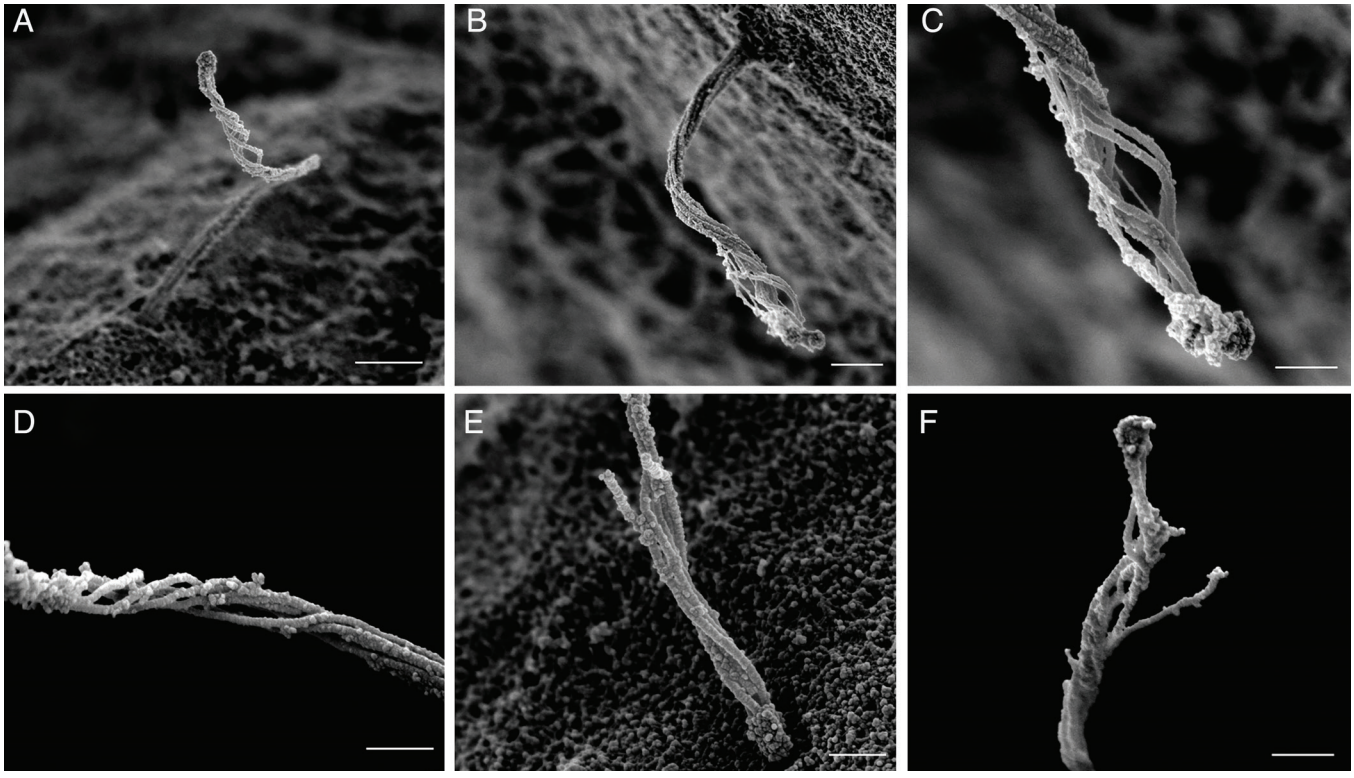

Fig. 7. Microtubule configurations in the distal axoneme. In demembranated cilia, microtubules rotate and separate in the distal portion of the axoneme, creating a helical cage (*A-D*). Occasional actin-like thin filaments are seen coursing along the microtubules (*C*). Splaying of individual microtubule filaments is likely due to specimen damage (*E* and *F*). Scale, *A* and *B*, 500 nm; *C–F*, 300 nm.

multiple hair fibers emerge from the same follicle (50). As with differences observed in cilia tip morphology, these multicilia may represent either normal heterogeneity or aberrant variations among islet primary cilia, as the mechanisms governing centrosome duplication and ciliogenesis are yet unclear in human islets.

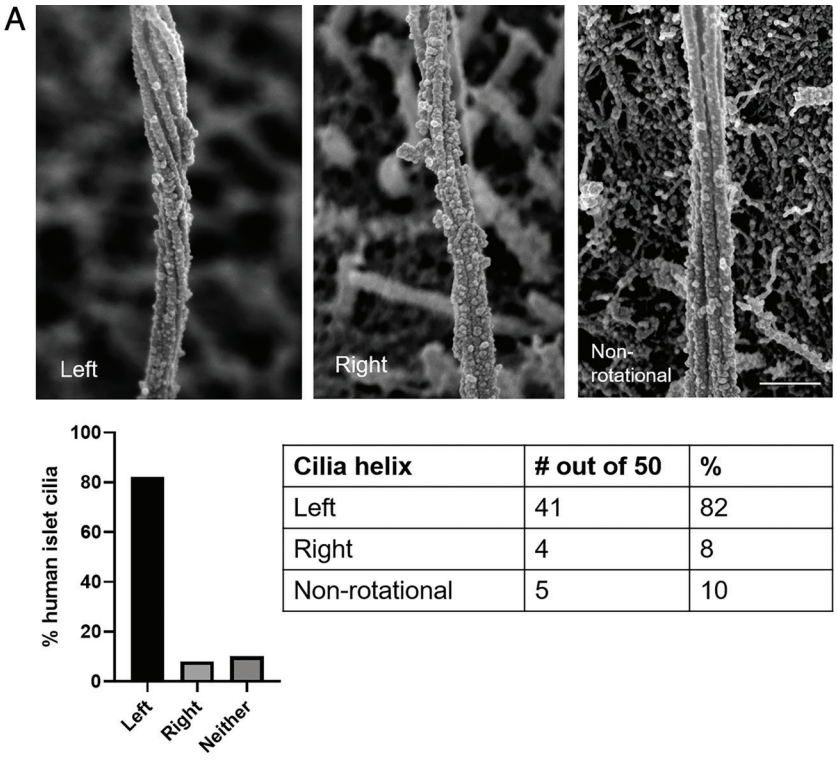

Cilia helix	# out of 50	%
Left	41	82
Right	4	8
Non-rotational	5	10

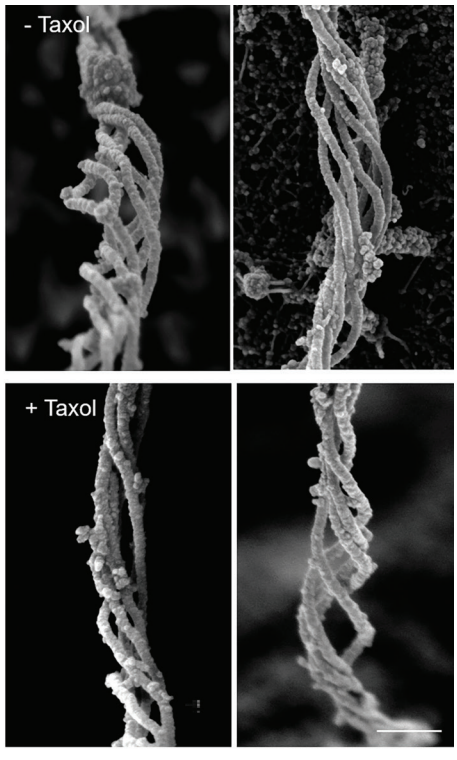

Fig. 8. Cilia handedness in human islets. Primary cilia in human islets exhibit chirality in the microtubule bundle, examples shown in (*A*) from mid-axoneme where rotations begin. Quantitation among 50 membrane-extracted cilia shows that the majority have left-handed turns, while a small minority have right-handed turns or no appreciable rotation. (Scale, 300 nm.) (*B*) The rotational nature of islet cilia is not altered by the microtubule-stabilizer taxol; shown are two representative images each of ± 1 μM taxol, distal axoneme where rotation is most pronounced. (Scale, 200 nm.)

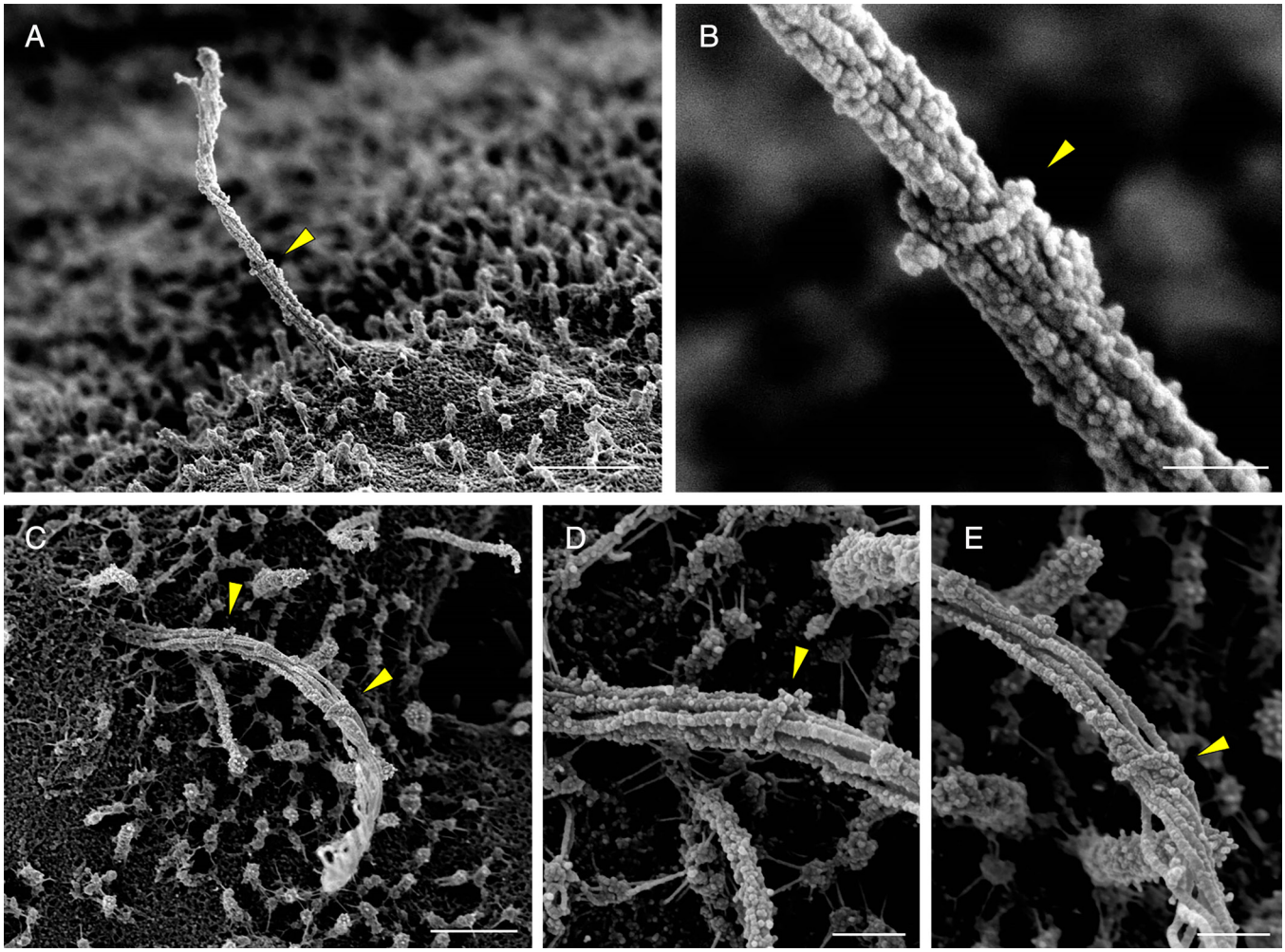

Fig. 9. A ciliary ring encircles the axoneme. Ring-like structures found on human beta cell cilia, shown here from different vantage points and marked by arrowheads (*A-E*). Note the contrasting cilia morphology proximal versus distal to the ring, where the ring location marks where the axonemal bundle begins to unwind and twist. (*B*, *D*, and *E*) are high-magnification views of (*A*, *C*). Scale, (*A*, *C*) 1 μm; (*B*, *D*, and *E*) 200 nm.

Discussion

Our data provide the highest-resolution view to-date of human primary cilia in any tissue and organ system. Recent advances in volumetric electron microscopy including focused ion beam scanning electron microscopy (FIB-SEM) and electron tomography (ET) has allowed 3D examinations of mammalian primary cilia including in rodent islets (15, 20, 22); however, no human islet data are available from these approaches. Our study fills this important gap, combining 3D approaches to visualize cilia in situ and multiscale imaging to resolve the full ciliary axoneme. The SEM protocol works reliably for fresh human donor islets and generates images suitable for both qualitative and quantitative analyses. We did observe some attrition in cilia number during the workflow, including islet loss from coverslips, cilia breaking off during specimen preparation, and sample charging during image acquisition, which are practical matters to keep in mind when adopting this imaging method. Nonetheless, among islets from three healthy male donors, we identified a robust number of cilia including 60 with full-length axoneme, which will serve as a reference dataset for future studies of islet cilia from patients with clinical disorders. Some key limitations and implications of our work are discussed below.

An important question that we could not formally address is the heterogeneity of cilia morphology among islet alpha/beta/delta cells. The identification of islet cell types, while a simple task by light microscopy and TEM, are trickier on SEM as there are not many identifying features unequivocally established for endocrine cell groups. We attempted to classify cells by surface morphology, relying on ultrastructural features reported by previous studies of human islets (23, 51, 52). For example, beta cells are known to express abundant microvilli (53, 54), which corresponded to a characteristic velvety appearance on their surface (Figs. 2 and 9). Alpha cells, in contrast, have smoother surfaces that are largely devoid of microvilli (Figs. 2*C* and 4*D*). Delta cells in human islets tend to be elongated and form long filopodial extensions (55), but whether they possess microvilli and whether these correspond to the much longer villi (Figs. 4*F* and 6*B*) than those observed on beta cells remains a question. Cellular abundance and distribution offer helpful clues, as the surface of human islets contains intermingling beta, alpha, and delta cells in roughly 5:3:1 ratio (51). Among the 60 cilia that were sampled in entirety in our dataset, we putatively identified 37 beta, 8 alpha, and 3 delta cells based on the postulation that beta cells express uniform short microvilli, alpha cells have few or no microvilli, and delta cells are rare cells with long villi. In other cases, the surface morphology was not clearly visualized to allow cell type identification. This was a limitation in our dataset that can be addressed by future studies where true cell identity might be ascertained by immuno-SEM or correlative light and electron microscopy using hormonal or cell

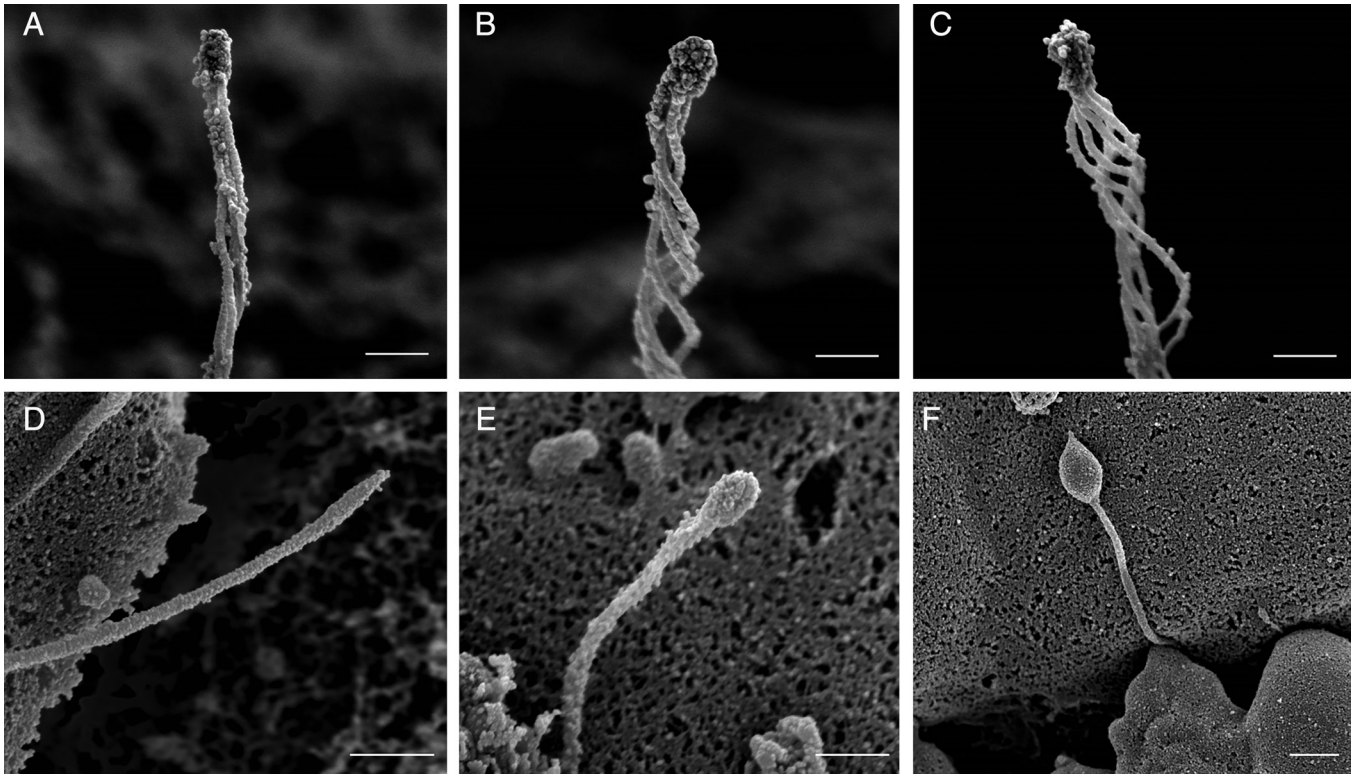

Fig. 10. Diversity of cilia tip morphology in human islet cells. (*A*–*C*) Demembranation reveals a conserved central microtubule organization where the microtubule filaments coalesce and terminate at a dense tip complex. The number of microtubules present at the tip is usually between 3 and 5. (*D* and *F*) Unextracted samples with intact ciliary membrane show greater heterogeneity including ciliary bulbs and bulges. Scale, *A*–*C*, 300 nm; *D*–*F*, 400 nm.

surface protein markers. Elemental analysis using energy dispersive X-ray spectroscopy (EDS/EDX) is another possibility, which could be used to identify islet cell type by relative abundance of phosphorus, sulfur, and nitrogen, corresponding to alpha, beta, and delta cell secretory granules (23, 52).

The arrangement of actin-like connections at the ciliary base offers clues to the role of actin in cilia dynamics. The ciliary pocket has been described to be a docking site for actin cables (28, 56, 57), where interactions between the actin cortex and the cilium may serve to either stabilize cilia or generate forces to influence cilia movement (40, 58, 59). The asymmetry and sometimes one-sidedness of these fibers observed in our SEM data (Fig. 4 *A*–*C*) suggest that they may act as cables to pull the cilium via extraciliary forces, akin to a model proposed by Lippincott–Schwartz and colleagues (40). Such forces may contribute to primary cilia motility in addition to intraciliary microtubule-dynein activities (16, 40). Other potential functions of actin and associated myosin at the cilia base include regulation of ciliogenesis, establishment of cilia orientation, and regulation of endocytic uptake, as demonstrated in several experimental systems (58, 60–64). The observation of actin-like filaments along the central axonemal axis (Fig. 7*C*) suggests that ciliary

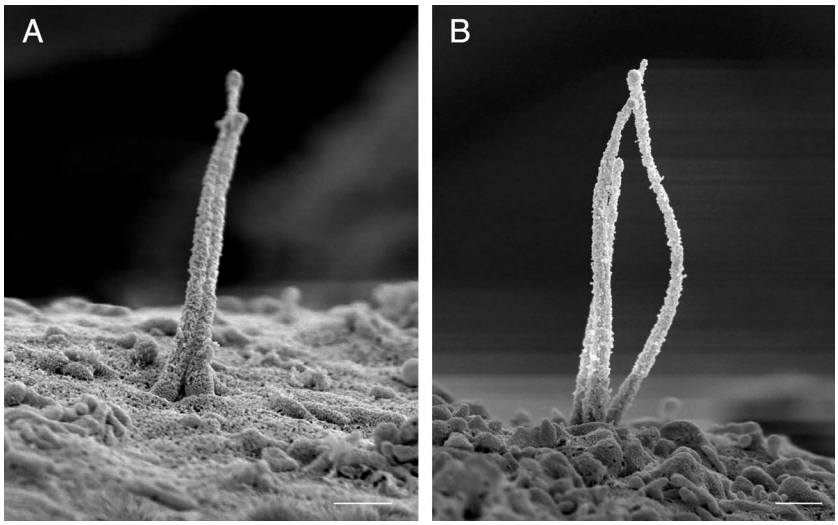

Fig. 11. Multicilia in human islet cells. (*A*) Double cilia emanating from a single enlarged pocket with two parallel axonemes similar in length and diameter, both possessing defined tips. (*B*) Three axonemes sharing a connected base, physically uncoupled but interactive in their tip regions. (Scales, 500 nm.) Minor background distortion is seen in both images from charge build-up during scanning.

actin could be a constitutive component that provides mechanical stability to the axoneme or partitions the cilia into functional microdomains, as has been proposed for non-islet cilia (19, 39). It would be informative to test these models experimentally in islet cells.

The helical nature and chirality of axonemal microtubules was an unexpected feature that may have functional significance. Our finding that islet cilia are mainly L-handed helices contrasts with earlier reports in kidney cell cilia, which produce mild R-handed spirals (19, 21). Centriolar triplets typically exhibit an anticlockwise spin in most tissues (65–67). If such a rotation were continued along microtubule doublets and singlets, this would indeed translate to a L-handed axoneme. While the functional difference of L- versus R-handed turns is yet unclear, we could at least conclude that cilia handedness can differ among cells, and speculatively, we may propose that it could differ among the same cell type under different growing conditions, a phenomenon well-described in the *Arabidopsis* plant (68). The more fundamental question is, what is the function of coiling? In contrast to tubulin protofilaments in which curved tips are thought to facilitate individual strand growth (69), collective coiling by the microtubule bundle likely contributes to overall axonemal stability and dynamics, acting as a compression shock absorber and a stretch and length modulator. With the microtubules fixed at both base and tip, the ciliary axoneme can be considered a topologically closed system, where changes in its helical conformation would allow elastic deformation without breaking strands of the microtubule bundle. In other words, the helical unwinding would be a quick way to increase ciliary length without polymerizing new subunits, and theoretically permit coil direction switching. Additionally, having loose microtubule helices in the distal axoneme would produce greater cilia surface area and luminal volume, which may alter the capacity for ciliary signaling, cargo trafficking, and exocytic vesicle release. However, as the degree of microtubule separation may be related to demembranation, it would be prudent to confirm these observations using more precise methods such as cryo-ET, which keeps tissues in a more accurate native state.

Among the most intriguing observations from our dataset is the "ciliary ring," previously not described in any mammalian primary cilia. The low frequency of the ring suggests that it may not always assemble, or survive demembranation as in our procedure. Ring complexes around individual microtubules have been reported in budding yeast (70), namely the Dam1 complex that aids in microtubule stability, but key differences are that 1) Dam1 ring thickness is about the size of tubulin protofilaments (~5 nm), thinner than that of a microtubule (25 nm), 2) Dam1 rings wrap around a single microtubule, whereas the ring observed on islet cilia wraps the entire axoneme bundle, and 3) Dam1 rings are not seen in other fungal species besides budding yeast nor in higher organisms, thus unlikely to represent the ring feature observed in this study. The ciliary ring that we describe is also distinct from the ciliary necklace and bracelet, which have different morphology and localization, for example the ciliary bracelet has only been observed in the flagella of the unicellular green alga *Chlamydomonas* (32). Nor does it resemble the gamma-tubulin rings reported in *Xenopus*, whose function is to cap the minus end and block MT growth (71). The only known ring-like structure that wraps around the entire axoneme is the membrane-bound septin ring at the cilium base (72). Septins are a family of guanosine-5'-triphosphate-binding proteins that act as diffusion barriers, and in primary cilia the septin ring is found below the transition zone. Thus location-wise, the septin ring is too low to be the structure that we observe, which is microns above the cell surface. While the composition of the ring remains unknown, we suggest based on its morphological resemblance to microtubules that this could be a tubulin-based complex that contributes to the structural integrity of the axoneme. Having a mid-axonemal ring could support microtubule bundling, promote cilia assembly, and stabilize against disassembly. Future studies might clarify the prevalence of the ring as well as regulatory factors in its formation. Whether the ring is fixed in place or could slide to dynamically control axonemal architecture or helical cage diameter is another interesting biomechanical question, but beyond the scope of this study.

Finally, the observation of compound primary cilia raises questions about their purpose and the mechanism of numerical control. The majority of cells in human pancreatic islets contain a single primary cilium, consistent with the idea that there may exist evolutionary mechanisms to ensure single primary cilia number for proper function (73). While our images clearly demonstrate the existence of double and triple cilia, we do not know their functional significance, nor can we glean from surface scans their anatomical origin, for example whether they are joined together at the basal body or accompanied by extranumerary centrioles. The Polo-like kinase (PLK) family proteins are well-studied regulators for centriole biogenesis in human cancer cell lines, with PLK4 being an established driver of centrosome duplication (74–76). While these pathways have not been experimentally studied in pancreatic islets, our survey of published human single-cell RNAseq datasets (77, 78) shows that all Plk1-5 genes including Plk4 have detectable and cell type-dependent expression in healthy human islets, suggesting that there indeed exist mechanisms for regulated cilia/centrosome duplication. The multicilia observed in our study were healthy-appearing, with normal lengths and diameters and individual ciliary membranes, surrounded by a well-formed ciliary pocket. Thus we posit that, rather than being a diseased oddity, these multicilia may be a normal feature among islet cells, perhaps retained over evolution to maintain cilia density per unit surface area or volume. Given the heterogeneity of Plk gene expression, multiciliation may also be differentially regulated among islet cell subsets or be under hormonal control. Gain- and loss-of-function studies in the future might demonstrate a role for PLK or related factors in centrosome amplification, cilia biogenesis, and islet function.

Methods

Islet Preparation for SEM. Human islets were obtained from the Integrated Islet Distribution Program (IIDP). After retrieving islets from the shipping bottle, we washed and rested islets overnight in islet medium [RPMI 1640 with 11 mM glucose, 10% FBS, and 1% Penicillin–Streptomycin (Gibco, #15140122)]. Islets were then plated on laminin-coated coverslips (treated with 0.5 μg laminin/cm^2 for 2 h), and allowed to adhere for 3 d. For fixation/extraction, islets were washed three times in phosphate-buffered saline (PBS), then membrane-extracted with successive incubations, first for 5 min in cytoskeleton buffer (50 mM imidazole, 50 mM KCl, 0.5 mM MgCl2, 0.1 mM EDTA, 1 mM EGTA, pH 6.8) with 0.5% Triton X-100 and 0.25% glutaraldehyde, then extracted for 10 min in cytoskeleton buffer with 2% Triton X-100 and 1% CHAPS, with or without 1 μM taxol (Cell Signaling #9807). Islets were washed three times in cytoskeleton buffer before fixation overnight in a solution containing 2% glutaraldehyde in 0.15 M cacodylate buffer, pH 7.4 at 4 °C.

SEM. Coverslips containing adhered and fixed islets were transferred into 0.1% tannic acid in ultrapure water for 20 min at room temperature. Following this, samples were rinsed four times for 5 min each in ultrapure water and incubated in 0.2% aqueous uranyl acetate for 20 min. Samples were rinsed three times for 10 min each in ultrapure water and dehydrated in a graded ethanol series (10%, 20%, 30%, 50%, 70%, 90%, and 100% ×3) for 5 min in each step. Once dehydrated, samples were loaded into a critical point drier (Leica EM CPD 300), which was set to perform 12 CO_2 exchanges at the slowest speed. Samples were

then mounted on aluminum stubs with carbon adhesive tabs and coated with 5 nm carbon and 5 nm iridium (Leica ACE 600). SEM images were acquired on a FIB-SEM platform (Helios 5 UX DualBeam Fisher Scientific, Brno, Czech Republic) using the SEM imaging mode at 1.8 kV and 0.1 nA using a TLD detector. False coloring was rendered in Adobe Photoshop. To promote data accessibility and sharing, original high-resolution TIFF images from this study have been deposited at the public database BioImage Archive https://www.ebi.ac.uk/biostudies/BioImages/studies, accession #S-BIAD664 (79).

Immunohistochemistry, Confocal and Superresolution Microscopy. Isolated human islets were washed with PBS and fixed with 4% paraformaldehyde (PFA) for 15 min and permeabilized with 0.3% Triton X-100 in PBS (phosphate-buffered saline with Triton X, PBST) for 10 min at room temperature. After incubation with blocking buffer (PBS with 10% normal goat serum) for 1 h at room temperature, islets were incubated overnight at 4 °C with primary antibodies diluted in PBST. Primary antibodies included mouse-anti-acetylated tubulin (Proteintech #66200-1-Ig, 1:400 dilution), rabbit-anti-ARL13b (Proteintech, 1:400 dilution), and mouse-anti-DNAIC1 (NeuroMab #75-372, 1:500 dilution). The next day, islets were washed, incubated with secondary antibodies for 1 h at room temperature, and washed again in PBST. DAPI provided nuclear counterstain. Islets were mounted on glass slides with Prolong Gold Anti-fade (Thermo Fisher P36930) and imaged using an inverted Zeiss LSM880 and Ti2 Eclipse SIM microscope on Airyscan mode (Nikon, Ti-E).

Morphometric Analysis. Linear measurements of human islet cilia length and diameter were performed in ImageJ using the straight line or freehand line measurement tool. Intact full-length cilia images were selected for analysis, excluding those that were fragmented or disrupted during sample processing. Results were compiled in GraphPad Prism and calculated for average and SD. Volume (V) and surface area (SA) calculations are derived by approximating the shape of the primary cilium to a truncated cone with base radius r_1 and tip radius r_2, or a right cylinder with radius r, and height h, using the following equations:

For a circular truncated cone:

$$\text{Volume: } V = \frac{1}{3\pi}\left(r_1^{\,2} + r_1 r_2 + r_2^{\,2}\right)h,$$

$$\text{Lateral area: } F = \pi\ \left(r_1 + r_2\right)\sqrt{\left[\left(r_1 + r_2\right)^2 + h^2\right]},$$

$$\text{Surface area: } S = F + \pi r_2^{\,2}.$$

For a uniform right cylinder:

$$V = \pi r^2 h,$$

$$SA = 2\pi rh + \pi r^2.$$

Data, Materials, and Software Availability. Imaging data have been deposited in BioImage Archive (https://www.ebi.ac.uk/biostudies/bioimages/studies/S-BIAD664 Accession #S-BIAD664) (79). All study data are included in the main text.

ACKNOWLEDGMENTS. We are indebted to Dr. Ursula Goodenough along with Dr. Bob Schmidt, Robyn Roth, and the WashU Cilia Group for help with data interpretation. We acknowledge the assistance of Drs. James Fitzpatrick and Praveen Krishnamoorthy at the Washington University Center for Cellular Imaging in electron and light microscopy studies, supported by Washington University School of Medicine, The Children's Discovery Institute of Washington University and St. Louis Children's Hospital (CDI-CORE-2015-505 and CDI-CORE-2019-813), the Foundation for Barnes-Jewish Hospital (3770) and the Washington University Diabetes Research Center (DK020579). Human pancreatic islets were provided by the NIDDK-funded Integrated Islet Distribution Program (IIDP) (RRID:SCR_014387) at City of Hope, NIH grant #2UC4DK098085 and the JDRF-funded IIDP Islet Award Initiative. A.J.P. is supported by the Diabetes and Related Metabolic Diseases training grant T32DK007120. Other funding included NIH grants DK115795 and DK127748 to J.W.H., Doris Duke Charitable Foundation grant DDFRCS to J.W.H., and DK115972 and DK123301 to D.W.P. Graphics were created with BioRender.com.

1. B. L. Munger, A light and electron microscopic study of cellular differentiation in the pancreatic islets of the mouse. *Am. J. Anat.* **103**, 275–311 (1958).
2. L. Boquist, Cilia and vesicular particles in the endocrine pancreas of the Mongolian gerbil. *J. Cell Biol.* **45**, 532–541 (1970).
3. N. A. Zaghloul, N. Katsanis, Mechanistic insights into Bardet-Biedl syndrome, a model ciliopathy. *J. Clin. Invest.* **119**, 428–437 (2009).
4. M. Fliegauf, T. Benzing, H. Omran, When cilia go bad: Cilia defects and ciliopathies. *Nat. Rev. Mol. Cell Biol.* **8**, 880–893 (2007).
5. J. L. Badano, N. Mitsuma, P. L. Beales, N. Katsanis, The ciliopathies: An emerging class of human genetic disorders. *Annu. Rev. Genomics Hum. Genet.* **7**, 125–148 (2006).
6. S. Lodh, E. A. O'Hare, N. A. Zaghloul, Primary cilia in pancreatic development and disease. *Birth Defects Res. C Embryo Today Rev.* **102**, 139–158 (2014).
7. P. DiIorio, A. R. Rittenhouse, R. Bortell, A. Jurczyk, Role of cilia in normal pancreas function and in diseased states. *Birth Defects Res. C Embryo Today Rev.* **102**, 126–138 (2014).
8. M. Titlbach, K. Fält, S. Falkmer, Postnatal maturation of the islets of Langerhans in sheep. Light microscopic, immunohistochemical, morphometric, and ultrastructural investigations with particular reference to the transient appearance of argyrophil insulin immunoreactive cells. *Diabetes Res.* **2**, 5–15 (1985).
9. M. Yamamoto, K. Kataoka, Electron microscopic observation of the primary cilium in the pancreatic islets. *Arch. Histol. Jpn.* **49**, 449–457 (1986).
10. N. Ashizawa, N. Hamamoto, T. Kaji, M. Watanabe, Scanning electron microscope examination of pancreatic ducts in stroke-prone spontaneously hypertensive rats (SHRSP). *Int. J. Pancreatol.* **22**, 51–57 (1997).
11. A. A. Aughsteen, The ultrastructure of primary cilia in the endocrine and excretory duct cells of the pancreas of mice and rats. *Eur. J. Morphol.* **39**, 277–283 (2001).
12. T. Iwanaga, T. Miki, H. Takahashi-Iwanaga, Restricted expression of somatostatin receptor 3 to primary cilia in the pancreatic islets and adenohypophysis of mice. *Biomed. Res.* **32**, 73–81 (2011).
13. M. H. Greider, D. W. Elliott, Electron microscopy of human pancreatic tumors of islet cell origin. *Am. J. Pathol.* **44**, 663–678 (1964).
14. E. A. Phelps *et al.*, Advances in pancreatic islet monolayer culture on glass surfaces enable super-resolution microscopy and insights into beta cell ciliogenesis and proliferation. *Sci. Rep.* **7**, 45961 (2017).
15. W. J. Gan *et al.*, Cell polarity defines three distinct domains in pancreatic β-cells. *J. Cell Sci.* **130**, 143–151 (2017).
16. J. H. Cho *et al.*, Islet primary cilia motility controls insulin secretion. *Sci. Adv.* **8**, eabq8486 (2022).
17. Z. A. Li, J. H. Cho, L. G. Woodhams, J. W. Hughes, Fluorescence imaging of beta cell primary cilia. *Front. Endocrinol.* **13**, 1004136 (2022), 10.3389/fendo.2022.1004136.
18. T. Caspary, C. E. Larkins, K. V. Anderson, The graded response to sonic hedgehog depends on cilia architecture. *Dev. Cell.* **12**, 767–778 (2007).
19. P. Kiesel *et al.*, The molecular structure of mammalian primary cilia revealed by cryo-electron tomography. *Nat. Struct. Mol. Biol.* **27**, 1115–1124 (2020).
20. C. S. Xu *et al.*, An open-access volume electron microscopy atlas of whole cells and tissues. *Nature* **599**, 147–151 (2021).
21. S. Sun, R. L. Fisher, S. S. Bowser, B. T. Pentecost, H. Sui, Three-dimensional architecture of epithelial primary cilia. *Proc. Natl. Acad. Sci. U.S.A.* **116**, 9370–9379 (2019).
22. A. Müller *et al.*, 3D FIB-SEM reconstruction of microtubule–organelle interaction in whole primary mouse β cells. *J. Cell Biol.* **220**, e202010039 (2020).
23. P. de Boer *et al.*, Large-scale electron microscopy database for human type 1 diabetes. *Nat. Commun.* **11**, 2475 (2020).
24. J. W. Hughes *et al.*, Primary cilia control glucose homeostasis via islet paracrine interactions. *Proc. Natl. Acad. Sci. U.S.A.* **117**, 8912–8923 (2020), 10.1073/pnas.2001936117.
25. C.-T. Wu *et al.*, Discovery of ciliary G protein-coupled receptors regulating pancreatic islet insulin and glucagon secretion. *Genes Dev.* **35**, 1243–1255 (2021).
26. M. V. Nachury, How do cilia organize signalling cascades? *Philos. Trans. R. Soc. Lond. B. Biol. Sci.* **369**, 20130465 (2014).
27. A. Fujioka *et al.*, Dynamics of the Ras/ERK MAPK cascade as monitored by fluorescent probes. *J. Biol. Chem.* **281**, 8917–8926 (2006).
28. A. Benmerah, The ciliary pocket. *Curr. Opin. Cell Biol.* **25**, 78–84 (2013).
29. R. Ghossoub, A. Molla-Herman, P. Bastin, A. Benmerah, The ciliary pocket: A once-forgotten membrane domain at the base of cilia. *Biol. Cell.* **103**, 131–144 (2011).
30. S. Sorokin, Centrioles and the formation of rudimentary cilia by fibroblasts and smooth muscle cells. *J. Cell Biol.* **15**, 363–377 (1962).
31. B. G. Barnes, Ciliated secretory cells in the pars distalis of the mouse hypophysis. *J. Ultrastruct. Res.* **5**, 453–467 (1961).
32. N. B. Gilula, P. Satir, The ciliary necklace. A ciliary membrane specialization. *J. Cell Biol.* **53**, 494–509 (1972).
33. E. Tani, K. Ikeda, M. Nishiura, N. Higashi, Specialized intercellular junctions and ciliary necklace in rat brain. *Cell Tissue Res.* **151**, 57–68 (1974).
34. C. Torikata, The ciliary necklace–A transmission electron microscopic study using tannic acid-containing fixation. *J. Ultrastruct. Mol. Struct. Res.* **101**, 210–214 (1988).
35. J. F. Reiter, O. E. Blacque, M. R. Leroux, The base of the cilium: Roles for transition fibres and the transition zone in ciliary formation, maintenance and compartmentalization. *EMBO Rep.* **13**, 608–618 (2012).
36. Q. Hu, W. J. Nelson, Ciliary diffusion barrier: The gatekeeper for the primary cilium compartment. *Cytoskeleton* **68**, 313–324 (2011).
37. W. Breipohl, A. S. Mendoza, F. Miragall, Freeze-etching studies on the ciliary necklace in the rat and chick. *J. Anat.* **130**, 801–807 (1980).
38. H. van den Hoek *et al.*, In situ architecture of the ciliary base reveals the stepwise assembly of intraflagellar transport trains. *Science* **377**, 543–548 (2022).
39. S. Lee, H. Y. Tan, I. I. Geneva, A. Kruglov, P. D. Calvert, Actin filaments partition primary cilia membranes into distinct fluid corrals. *J. Cell Biol.* **217**, 2831–2849 (2018).
40. C. Battle, C. M. Ott, D. T. Burnette, J. Lippincott-Schwartz, C. F. Schmidt, Intracellular and extracellular forces drive primary cilia movement. *Proc. Natl. Acad. Sci. U.S.A.* **112**, 1410–1415 (2015).

41. P. Kohli *et al.*, The ciliary membrane-associated proteome reveals actin-binding proteins as key components of cilia. *EMBO Rep.* **18**, 1521–1535 (2017).
42. H. J. Hoops, G. B. Witman, Outer doublet heterogeneity reveals structural polarity related to beat direction in Chlamydomonas flagella. *J. Cell Biol.* **97**, 902–908 (1983).
43. C. L. Williams *et al.*, MKS and NPHP modules cooperate to establish basal body/transition zone membrane associations and ciliary gate function during ciliogenesis. *J. Cell Biol.* **192**, 1023–1041 (2011).
44. S. K. Dutcher, E. T. O'Toole, The basal bodies of Chlamydomonas reinhardtii. *Cilia* **5**, 18 (2016).
45. R. L. Weiss, D. A. Goodenough, U. W. Goodenough, Membrane particle arrays associated with the basal body and with contractile vacuole secretion in Chlamydomonas. *J. Cell Biol.* **72**, 133–143 (1977).
46. P. M. Andrews, K. R. Porter, A scanning electron microscopic study of the nephron. *Am. J. Anat.* **140**, 81–115 (1974).
47. A. S. Shah *et al.*, Loss of Bardet-Biedl syndrome proteins alters the morphology and function of motile cilia in airway epithelia. *Proc. Natl. Acad. Sci. U.S.A.* **105**, 3380–3385 (2008).
48. Y. Hou, G. J. Pazour, G. B. Witman, A dynein light intermediate chain, D1bLIC, is required for retrograde intraflagellar transport. *Mol. Biol. Cell* **15**, 4382–4394 (2004).
49. D. Huangfu, K. V. Anderson, Cilia and hedgehog responsiveness in the mouse. *Proc. Natl. Acad. Sci. U.S.A.* **102**, 11325–11330 (2005).
50. L. Lester, C. Venditti, The prevalence of pili multigemini. *Br. J. Dermatol.* **156**, 1362–1363 (2007).
51. M. Brissova *et al.*, Assessment of human pancreatic islet architecture and composition by laser scanning confocal microscopy. *J. Histochem. Cytochem.* **53**, 1087–1097 (2005).
52. P. de Boer, B. N. Giepmans, State-of-the-art microscopy to understand islets of Langerhans: What to expect next? *Immunol. Cell Biol.* **99**, 509–520 (2021).
53. E. Geron, S. Boura-Halfon, E. D. Schejter, B.-Z. Shilo, The edges of pancreatic islet β cells constitute adhesive and signaling microdomains. *Cell Rep.* **10**, 317–325 (2015).
54. L. Orci, B. Thorens, M. Ravazzola, H. F. Lodish, Localization of the pancreatic beta cell glucose transporter to specific plasma membrane domains. *Science* **245**, 295–297 (1989).
55. R. A. Drigo *et al.*, Structural basis for delta cell paracrine regulation in pancreatic islets. *Nat. Commun.* **10**, 1–12 (2019).
56. A. Molla-Herman *et al.*, The ciliary pocket: An endocytic membrane domain at the base of primary and motile cilia. *J. Cell Sci.* **123**, 1785–1795 (2010).
57. J. B. Rattner, P. Sciore, Y. Ou, F. A. van der Hoorn, I. K. Y. Lo, Primary cilia in fibroblast-like type B synoviocytes lie within a cilium pit: A site of endocytosis. *Histol. Histopathol.* **25**, 865–875 (2010).
58. B. Mitchell, R. Jacobs, J. Li, S. Chien, C. Kintner, A positive feedback mechanism governs the polarity and motion of motile cilia. *Nature* **447**, 97–101 (2007).
59. I. Antoniades, P. Stylianou, P. A. Skourides, Making the connection: Ciliary adhesion complexes anchor basal bodies to the actin cytoskeleton. *Dev. Cell* **28**, 70–80 (2014).
60. M. Lemullois, C. Klotz, D. Sandoz, Immunocytochemical localization of myosin during ciliogenesis of quail oviduct. *Eur. J. Cell Biol.* **43**, 429–437 (1987).
61. E. Boisvieux-Ulrich, M.-C. Lainé, D. Sandoz, Cytochalasin D inhibits basal body migration and ciliary elongation in quail oviduct epithelium. *Cell Tissue Res.* **259**, 443–454 (1990).
62. W. F. Marshall, "Chapter 1 basal bodies: Platforms for building cilia" in *Current Topics in Developmental Biology in of Ciliary Function in Mammalian Development* (Academic Press, 2008), **vol. 85**, pp. 1–22.
63. J. Kim *et al.*, Functional genomic screen for modulators of ciliogenesis and cilium length. *Nature* **464**, 1048–1051 (2010).
64. V. Raghavan, Y. Rbaibi, N. M. Pastor-Soler, M. D. Carattino, O. A. Weisz, Shear stress-dependent regulation of apical endocytosis in renal proximal tubule cells mediated by primary cilia. *Proc. Natl. Acad. Sci. U.S.A.* **111**, 8506–8511 (2014).
65. R. Uzbekov, C. Prigent, Clockwise or anticlockwise? Turning the centriole triplets in the right direction! *FEBS Lett.* **581**, 1251–1254 (2007).
66. P. Gönczy, Towards a molecular architecture of centriole assembly. *Nat. Rev. Mol. Cell Biol.* **13**, 425–435 (2012).
67. P. Satir, Chirality of the cytoskeleton in the origins of cellular asymmetry. *Philos. Trans. R. Soc. Lond. B. Biol. Sci.* **371**, 20150408 (2016).
68. S. Thitamadee, K. Tuchihara, T. Hashimoto, Microtubule basis for left-handed helical growth in Arabidopsis. *Nature* **417**, 193–196 (2002).
69. R. Orbach, J. Howard, The dynamic and structural properties of axonemal tubulins support the high length stability of cilia. *Nat. Commun.* **10**, 1838 (2019).
70. S. Westermann *et al.*, Formation of a dynamic kinetochore- microtubule interface through assembly of the Dam1 ring complex. *Mol. Cell* **17**, 277–290 (2005).
71. Y. Zheng, M. L. Wong, B. Alberts, T. Mitchison, Nucleation of microtubule assembly by a γ-tubulin-containing ring complex. *Nature* **378**, 578–583 (1995).
72. Q. Hu *et al.*, A septin diffusion barrier at the base of the primary cilium maintains ciliary membrane protein distribution. *Science* **329**, 436–439 (2010).
73. M. R. Mahjoub, The importance of a single primary cilium. *Organogenesis* **9**, 61–69 (2013).
74. R. Habedanck, Y.-D. Stierhof, C. J. Wilkinson, E. A. Nigg, The Polo kinase Plk4 functions in centriole duplication. *Nat. Cell Biol.* **7**, 1140–1146 (2005).
75. J. Kleylein-Sohn *et al.*, Plk4-induced centriole biogenesis in human cells. *Dev. Cell* **13**, 190–202 (2007).
76. D. K. Breslow, A. J. Holland, Mechanism and regulation of centriole and cilium biogenesis. *Annu. Rev. Biochem.* **88**, 691–724 (2019).
77. S. Shrestha *et al.*, Combinatorial transcription factor profiles predict mature and functional human islet α and β cells. *JCI Insight* **6**, e151621 (2021).
78. J. Li *et al.*, Single-cell transcriptomes reveal characteristic features of human pancreatic islet cell types. *EMBO Rep.* **17**, 178–187 (2016).
79. A. J. Polino, S. Sviben, I. Melena, D. W. Piston, J. W. Hughes, Scanning electron microscopy of human islet primary cilia. Bioimage Archive. https://www.ebi.ac.uk/biostudies/bioimages/studies/S-BIAD664. Deposited 4 April 2023.